CDF/ANAL/ELECTROWEAK/PUBLIC/6884
Draft 3.1
May 25, 2004

Measurement of W and Z Production Cross Sections and Ratio in Muon Channel with 200 pb^{-1}

Alexei Varganov[1], Dan Amidei, Ken Bloom, Jian Kang
University of Michigan

Victoria Martin, Michael Schmitt
Northwestern University

Eric James
FNAL

Abstract

We present a new updated measurement of the ratio of inclusive W and Z boson cross sections in proton-antiproton collisions at 1.96 TeV at the Fermilab Tevatron, using high-P_T muons in the CDF detector. Our measurement yields:

$$\sigma(p\bar{p} \to W)BR(W \to \mu\nu) = 2.786^{+0.065}_{-0.055}(\text{syst}) \pm 0.012(\text{stat}) \pm 0.166(\text{lum}) \text{ nb},$$

$$\sigma(p\bar{p} \to Z)BR(Z \to \mu^+\mu^-) = 253.1^{+8.3}_{-6.4}(\text{syst}) \pm 4.2(\text{stat}) \pm 15.2(\text{lum}) \text{ pb},$$

$$R = 11.02^{+0.17}_{-0.14}(\text{syst}) \pm 0.18(\text{stat}).$$

A comparison with theoretical predictions allows an indirect value for the W leptonic branching ratio:

$$BR(W \to \mu\nu) = 11.01^{+0.17}_{-0.14}(\text{syst}) \pm 0.18(\text{stat}) \pm 0.05(\text{ext}) \ \%.$$

Using the Standard Model prediction for $\Gamma(W \to \ell\nu)$ we extract the total width of the W boson:

$$\Gamma(W) = 2056^{+26}_{-32}(\text{syst}) \pm 34(\text{stat}) \pm 10(\text{ext}) \text{ MeV}.$$

We discuss the significance of the ratio measurement in light of existing information on W and Z production and decay.

[1]varganov@fnal.gov

Contents

1 Introduction

Since the start of the CDF Run II data taking several measurements of inclusive W and Z boson productions cross section in the muon channel have been performed for various data volumes [1, 2, 3, 4]. The result presented in this note is based on much larger data sample, which allows us to reduce significantly both statistical and systematic uncertainties.

The $p\bar{p}$ production rate of W and Z bosons is described through the cross section quantity. The probability for these bosons to decay in a final state with a muon is defined as the branching ratio. We can express the product of the production cross section and the branching ratio for a vector boson decay in the muon channel in terms of the measured variables:

$$\sigma(p\bar{p} \to V) \cdot BR(V \to \mu X) = \frac{N - B}{A\epsilon \int Ldt} \ , \tag{1}$$

where: N — the number of candidate events passing the selection, B — the estimated number of background events, A — detector acceptance, ϵ — efficiency of the selection cuts, $\int Ldt$ — luminosity integral.

When taking the ratio of $p\bar{p}$ production cross section for W and Z in muon channel

$$R = \frac{\sigma(p\bar{p} \to W) \cdot BR(W \to \mu\nu)}{\sigma(p\bar{p} \to Z) \cdot BR(Z \to \mu\mu)} = \frac{\sigma(p\bar{p} \to W)}{\sigma(p\bar{p} \to Z)} \frac{\Gamma(W \to \mu\nu)}{\Gamma(W)} \frac{\Gamma(Z)}{\Gamma(Z \to \mu\mu)} \quad (2)$$

we can extract the value of the branching ratio $BR(W \to \mu\nu) = \Gamma(W \to \mu\nu)/\Gamma(W)$ using the theoretical calculation of the production cross sections and precise Z width measurements from LEP experiment [5]. This measurement promises high precision due to the fact that luminosity does not enter the expression. Also we expect complete or partial cancellation of many uncertainties in the ratio when the muon identification is the same both for W and Z selection. We can further extract the value W width parameter $\Gamma(W)$ using the Standard Model calculation for W leptonic width $\Gamma(W \to \ell\nu)$.

In this note we present a new updated measurement of the ratio R of inclusive W and Z boson cross sections in proton-antiproton collisions at 1.96 TeV using 193.5 pb^{-1} of high-P_T muon data collected by the CDF detector. We describe how different parameters entering Equation 1 are measured both for W and Z bosons. We also derive the values and uncertainties for acceptance and efficiency ratios that enter the Equation 2. At the end of the note we discuss the significance of the ratio measurement in light of existing information on W and Z production and decay.

2 Data Sets

The high-P_T muon data set used in these measurements was collected between March 23, 2002 and September 6, 2003 and has a corresponding run range of *141544* to *168889*. The Data Quality Monitoring working group established a common list of good runs [6] for leptons that is used to select events from this run range. The integrated luminosity for this run range is determined to be 193.5 $\pm$ 11.6 pb^{-1}.

This data has been collected through the high-P_T CMUP and CMX muon trigger paths, as described in Section 3, into the original data sample bhmu08, which is processed with the version `4.8.4` of the reconstruction code. To reduce the size of the data set it is stripped further into the intermediate multipurpose sample btop1g, which contains the sub-sample of events with a reconstructed muon that passes a loose set of muon identification cuts [7]. This data sample is refined further through a substantial amount of re-processing using version `4.11.2` of the offline reconstruction code [8]. The finalized sample is then registered under rtop01 data set name and put on tape through the CDF data file catalog system [9].

For the background and acceptance calculations we also used the samples of simulated events. These samples were generated using the `PYTHIA` [10] Monte Carlo generator with the `CTEQ5L` [11] parton distribution functions. The transverse motion of the vector boson and underlying event activity is tuned to match the data [4]. The full CDF simulation is used to model the detector response. The generated data sets wewk0m, wewk0t, zewk0m, zewk0t correspond to the processes $W \to \mu\nu$, $W \to \tau\nu$, $Z \to \mu\mu$, $Z \to \tau\tau$ respectively.

3 Inclusive High-P_T Muon Trigger Paths

The muon data set described in the previous section is written through the Stream B data channel, which is fed by high-P_T lepton trigger paths. Currently, there are two basic trigger paths for inclusive high-P_T muons: `MUON_CMUP18` and `MUON_CMX18`.

The `MUON_CMX18` data collected prior to run number *150145* is not used in physics analysis due to the large noise in CMX chambers. The combination of both trigger paths in our measurement may produce additional sources of uncertainties. On the other hand if we base our measurement solely on data gathered from `MUON_CMUP18` trigger path many parameters will cancel out completely, thus improving the overall result.

The `MUON_CMUP18` trigger path is divided into three levels:

- `L1_CMUP6_PT4`: The muon trigger cards attempt to match XFT track with both CMU and CMP hits. XFT provides tracks with $P_T \geq 4$ GeV/c and at least 10 hits per axial super layer. Starting from run *152612* the minimum number of hits per super layer becomes 11.

- `L2_TRK_L1_CMUP6_PT4`: Prior to run *152612* all events fed by Level 1 trigger were auto-accepted an sent further to Level 3. Starting from run *152612* events coming from Level 1 required to have a XFT track with $P_T \geq 8$ GeV/c in order to pass Level 2 trigger requirements.

- `L3_MUON_CMUP18`: The trigger code attempts to reconstruct muon COT track and links it to the CMU and CMP track segments or stubs. The required P_T of the COT track must be greater than 18 GeV/c. The code also checks matching between projected muon trajectory and stubs in the plane transverse to the beamline. The track must match stub within 10 *cm* for CMU and 30 *cm* for CMP chambers.

Every event in our sample must have at least one muon that triggered the event according to these requirements. Additional offline selections are described in more details in the next Section 4.

4 Muon Identification

For our event selection it is extremely important to reject backgrounds and retain high-P_T muons with very high efficiency. This can be achieved by cutting on numerous variables associated with the reconstructed particle. Within the analysis framework a muon is defined as a reconstructed object that consists of a track linked to the respective muon chamber track segments or stubs. Very often muons also traverse the calorimeter detector towers depositing typical minimum ionizing energy, leaving neighboring calorimeter towers unaffected. The collection of track, stub, and calorimeter tower parameters provides us with many variables that can be used for muon selection.

We insure the quality of muon object by enforcing the following requirements:

- the muon is represented by the high quality track
- the matching between muon track and muon chamber segments is good
- the energy for calorimiter towers near muon track is consistent with minimum ionizing deposition

Several requirements are introduced to select a good muon track. We only consider the tracks that will pass through at least eight COT super-layers, which means that muon exits the tracker end-plate at the radius ρ greater than 140 cm. Then, we ensure that track originates within the luminous beam region, which can be represented in terms of track helix parameters as:

$\mid z_0 \mid < 60\ cm$ — along the beam-line, and

$\mid d_0^{cor} = d_0 + x_{beam} \cdot sin(\phi) - y_{beam} \cdot cos(\phi) \mid < 0.2\ cm$ — in the transverse plane.

If silicon hits are present on the reconstructed track we require $\mid d_0^{cor} \mid < 0.02\ cm$. We also demand that track contains at least 3 good axial and 3 good stereo segments, where each good segment in turn has at least seven COT associated hits. The quality of track helix fit is ensured by requiring $\mid \chi^2_{COT}/ndf \mid < 2$, where the number of degree of freedom can be expressed through the number of associated COT hits on track $ndf = N^{hits}_{COT} - 5$.

The CMU and CMP stubs in the fiducial regions of muon chambers linked to the muon track are subject to the matching cuts, which is $|\Delta X|_{CMU} < 3\ cm$ for CMU chamber, and $|\Delta X|_{CMP} < 5\ cm$ for CMP chamber. Blue-beam section of CMP chambers was not operating during the normal data taking period. Therefore, in this note these detectors were considered as non-fiducial parts of CMP coverage.

The calorimeter response is divided into two parts: the energy from electromagnetic compartment and the energy from hadronic compartment. To take into account muon momentum dependence [12], the following criteria is used to insure minimum ionizing energy deposition in calorimeter towers:

$$E_{EM} < max\{2,\ 2 + 0.0115(E_\mu - 100)\} \text{ and } E_{HAD} < max\{6,\ 6 + 0.0280(E_\mu - 100)\},$$

where calorimeter E_{EM}, E_{HAD} and muon E_μ energies are measured in GeV. In this case muon energy E_μ is equal to the absolute value of muon momentum $|\vec{P}_\mu|$.

The muon isolation variable is defined as ratio of the measured E_T in a $\Delta R = 0.4$ cone centered on the muon track excluding the muon tower and divided by the muon P_T. Muons with a measured isolation ratio less than 0.1 are accepted into the event sample.

Events collected in our data sample must have at least one high-P_T muon with $P_T \geq 18$ GeV/c due to the trigger selections discussed in Section 3. For our analysis we slightly raise the value of the muon transverse momentum cut to make it $P_T \geq 20$ GeV/c to get rid of the hardware and software trigger resolution effects.

The technique used for vetoing cosmic rays is described in details the next Section 5.

The complete set of selections for inclusive high-P_T muon is summarized in Table 1.

Requirement	Purpose	Number of Passed Events
Good Run	Quality Data	1,128,370
Fiducial Muons	Muon Chamber Active Regions	727,865
Trigger Bits	Enforce Online Trigger	674,699
CMU and CMP Stubs	Use Central Muon Detectors	669,131
Cosmic Veto	Remove Cosmic Rays	491,023
$\|z_0\| < 60\ cm$	Nominal Collision Region	421,166
COT Radius $\rho \geq 140\ cm$	Fiducial Tracks	421,165,
$P_T \geq$20 GeV/c	Low-P_TNoise Reduction	246,681
$\|\Delta X\|_{CMU} < 3\ cm$	Good Stub-Track Match	190,729
$\|\Delta X\|_{CMP} < 5\ cm$	Good Stub-Track Match	153,598
$E_{EM} < 2$ GeV	Minimum Ionizing Deposition	143,313
$E_{HAD} < 6$ GeV	Minimum Ionizing Deposition	138,007
$N_{Seg}^{Ax} \geq 3$, $N_{Seg}^{St} \geq 3$	Good Track Quality	120,956
$\|d_0^{cor}\| < 0.2\ cm$	Good Track Quality	111,064
$\chi^2_{COT}/ndf < 2$	Good Track Quality	109,784
$Iso < 0.1$	Background Reduction	77,140

Table 1: Inclusive high-P_T muon selection cuts.

5 Cosmic Ray Contamination

Energetic cosmic ray muons traverse the detector at the significant rate, leaving hits in both muon and COT chambers and passing the high-P_T muon trigger requirements. Thus the original muon data set is heavily contaminated with the cosmic ray events.

A cosmic muon, passing through the detector, represents itself as a combination of incoming and outgoing legs relative to the beam line of the detector. To be recorded in the data, at least one such leg should form a good COT track with muon stubs linked to it. Often the other leg also gets reconstructed as a track or muon. The majority of events triggered by cosmic muons have much lower tracking multiplicity in comparison with the collision events. On the other hand, the fraction of events in which the cosmic muon hits the detector during the collision is quite significant.

Muons from cosmic rays are generally very isolated and easily pass the muon identification cuts listed in Table 1. When only one cosmic leg is reconstructed, the event can imitate the W signature. Quite often both cosmic legs are present and in this case the event fakes Z decay. Therefore, an effective cosmic tagging technique is required to reduce cosmic background in both parts of our data sample.

The cosmic ray tagging algorithm [13] utilizes the timing information of the COT hits. The core of this method is a multi-parameter fit over the set of hits left by the

incoming and outgoing cosmic legs. The leg belonging to the reconstructed muon serves as the seed track for the fit. The other leg is referred to as the opposite track.
The algorithm performs in the following steps:

- hits belonging to the seed track are refitted with the 5 helix parameters and the global time shift
- based on the best value of the fit, incoming or outgoing hypothesis is assigned to the seed track
- the refitted seed track is used to find the other cosmic leg by defining a "road" in which hits are searched for.
- if enough hits are found, a similar fit is performed to produce the opposite track
- for the seed and the opposite tracks a simultaneous fit is performed to combine all hits into a single helix

The final decision of the cosmic tagger depends on the assigned direction of the legs. If one leg is recognized as incoming and the other as outgoing, then the event is tagged as cosmic ray. For a pair of tracks coming out of a real beam collision, both legs should be categorized as outgoing.

Further details on the cosmic ray backgrounds and tagger efficiency will be described in Sections 7, 9, and 11 of this note.

6 W Selection Criteria

When W boson decays into muon and neutrino, the final state particles acquire high momentum due to a large W mass.

A kinematic cut $P_T \geq 20$ GeV/c is applied to the muon from W decay along with the other cuts that coincide with the inclusive selections described previously in more details in Section 4. The comparison of the muon transverse momentum spectrum between data and simulation for events passing W selection requirements is shown on Figure 1.

All muon momentum components can be reconstructed by COT, but there is no direct way to measure neutrino momentum components. We can, however, infer the transverse momentum of neutrino by measuring the *missing transverse energy* of the event. The $\hat{z}$-component of the neutrino momentum cannot be reconstructed, since for proton-antiproton collision the longitudinal momentum of interacting parton pair is unknown. Therefore, event kinematics can only be reconstructed in the transverse plane with respect to the beam-line direction.

To reconstruct the missing transverse energy of the event we first define the event's "total energy vector" $\vec{E}_T = (E_x, E_y)$ in the transverse plane

$$E_x = \sum_i (HAD_T^i + EM_T^i) cos\phi_i \qquad E_y = \sum_i (HAD_T^i + EM_T^i) sin\phi_i \ , \tag{3}$$

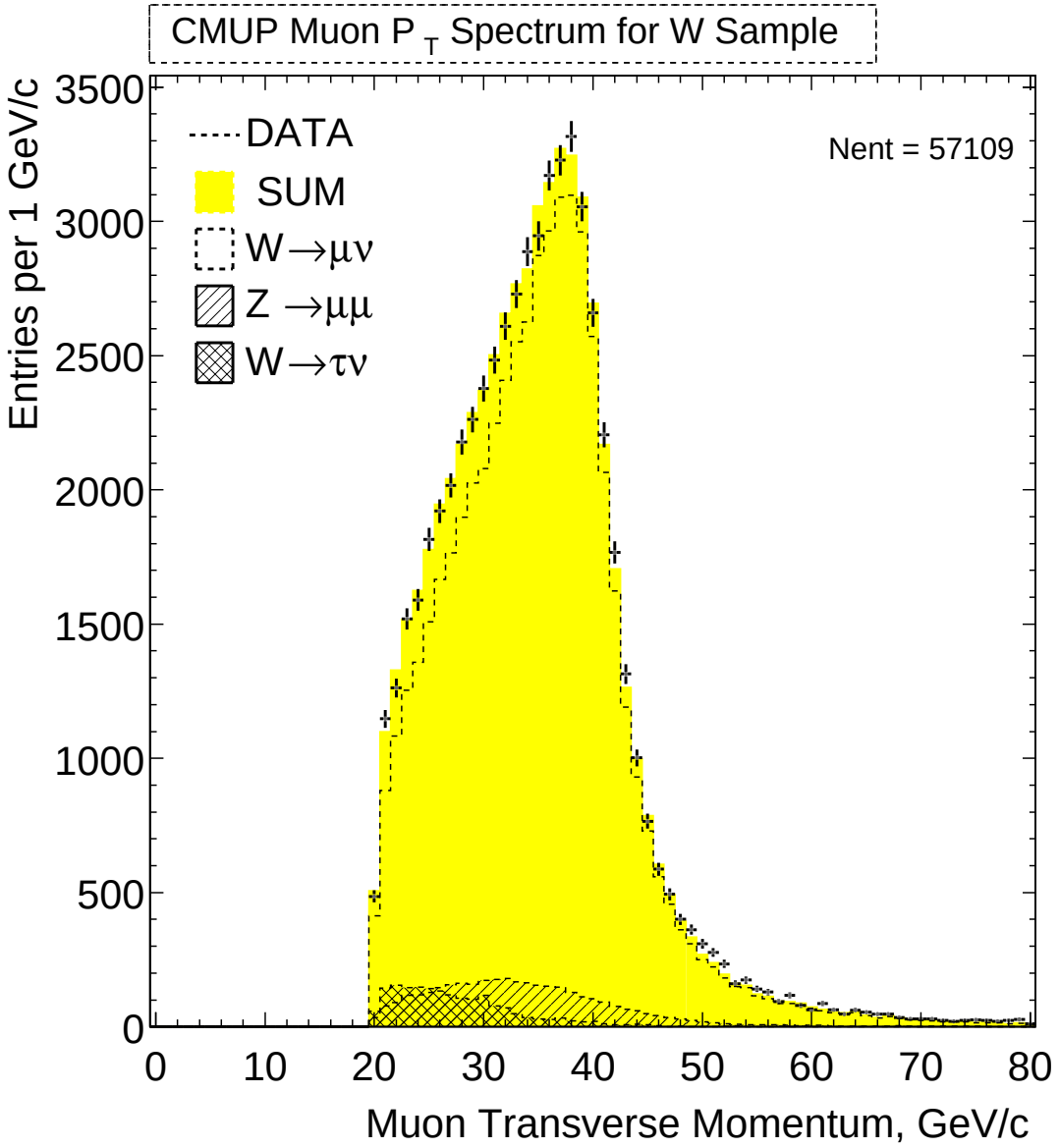

Figure 1: Muon transverse momentum spectrum in data and simulation for $W \to \mu\nu$ candidate events. Only the leading contributing processes are shown.

where HAD_T^i — the amount of energy deposited in the hadronic calorimeter tower i projected on transverse plane, EM_T^i — the amount of energy deposited in the electromagnetic calorimeter tower projected on transverse plane, ϕ_i — the polar angle of the calorimeter tower, and the sum is taken over all detector towers.

The colliding parton pair has zero initial momentum in the transverse plain, so using the conservation of momentum we define the missing transverse energy vector as

$$\vec{E}_T + \vec{\not{E}}_T = 0, \ \vec{\not{E}}_T = -\vec{E}_T \tag{4}$$

and we ascribe the absolute value of $\not\!\!E_T$ to the transverse momentum of the neutrino for events where one neutrino is expected.

When a muon is present in the event it deposits only minimum ionizing energy in the calorimeter. Therefore, for high-P_T muons the actual momentum in the event is much greater than the energy they deposit in the calorimeter towers. To make a correction for this case we exclude muon energy deposition and add its momentum contribution in the Equations 3

$$E_x = \sum_i (HAD_T^i + EM_T^i) cos\phi_i \ - (HAD_T^\mu + EM_T^\mu) cos\phi_\mu + P_T^\mu cos\phi_\mu \tag{5}$$

$$E_y = \sum_i (HAD_T^i + EM_T^i) sin\phi_i \ - (HAD_T^\mu + EM_T^\mu) sin\phi_\mu + P_T^\mu sin\phi_\mu \tag{6}$$

where HAD_T^μ — minimum ionizing energy deposited in the hadronic calorimeter tower traversed by muon projected on transverse plane, EM_T^μ — minimum ionizing energy deposited in the electromagnetic calorimeter tower traversed by muon projected on transverse plane, ϕ_μ — the polar angle of the muon, P_T^μ — muon transverse momentum.

Figure 9 shows the $\not\!\!E_T$ spectrum of simulated electroweak processes along with our model of the QCD background. The electroweak processes and the QCD background are relatively well separated. Therefore, to reject most of the non-electroweak background and retain the signal efficiently we chose a kinematic cut $\not\!\!E_T \geq 20$ GeV.

As will be shown in Section 7 the contamination from Z events is the leading source of background. To reduce $Z \to \mu\mu$ presence in W candidate events a special Z rejection criteria is applied. The events are rejected only if the second muon passes a loose set of minimum ionizing energy deposition cuts $EM < 3$ GeV and $HAD < 9$ GeV. This criteria guarantees that there is no more than one high-$P_T$muon-like object in the event, which also simplifies the $\not\!\!E_T$ calculation.

Table 2 summarizes the W selection cuts and lists the number of passed events at every stage of the selection. The detailed description of the inclusive muon selection is listed previously in Section 4.

Requirement	Purpose	Number of Passed Events
Inclusive Muon	High-P_T Quality Muon	77,140
Z Veto	Remove Z Events	70,512
$\not\!\!E_T > 20$ GeV	Background Reduction	57,109

Table 2: $W \to \mu\nu$ selection cuts.

Since the neutrino momentum is not fully reconstructible we cannot measure the dilepton invariant mass to constrain further the kinematics of the W candidate events. However, we can build dilepton *transverse mass* — a two dimensional analog of the invariant mass, constrained to the transverse plane:

$$M_T = \sqrt{(P_T^\mu + \not\!\!E_T)^2 - (\vec{P}_T^\mu + \vec{\not\!\!E}_T)^2} \ , \tag{7}$$

where $P_T^\mu = |\vec{P}_T^\mu|$ — absolute value of muon transverse momentum, and $\not\!\!E_T = |\vec{\not\!\!E}_T|$ — absolute value of missing transverse energy in the event.

The reconstructed transverse mass spectrum for W candidates is shown on Figure 2 both for data and simulation events. The distributions has the characteristic shape of the *Jacobian peak*, which has its maximum near the actual mass of W boson and rapidly falls off for the values above the W mass. At the values below the W mass the spectrum falls slowly until it drops at 40 GeV/c^2 — the kinematic limit imposed by our W selection cuts $P_T \geq$20 GeV/c and $\not\!\!E_T \geq$ 20 GeV.

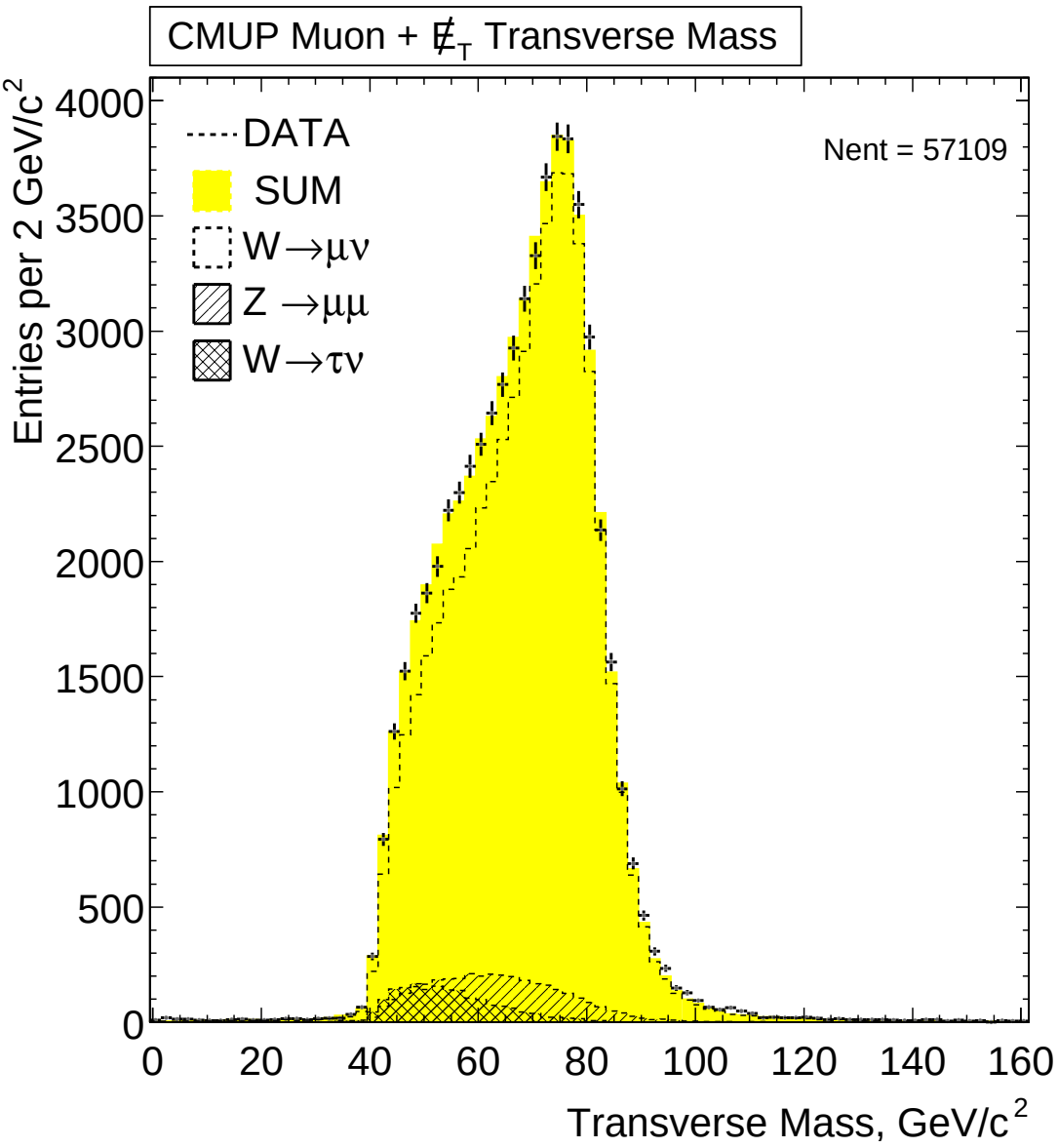

Figure 2: The transverse mass spectrum in data and simulation for $W \to \mu\nu$ events.

The yield of W candidate events for the data-taking runs is shown on Figure 3. The run interval is sampled in the ranges with the corresponding integrated luminosity of at least 8 pb^{-1}. Figure 4 shows W event count per inverse picobarn of delivered luminosity for various run ranges, which is a relatively flat distribution. Higher event count for the first four run ranges reflects the changes in muon trigger as previously described in Section 3.

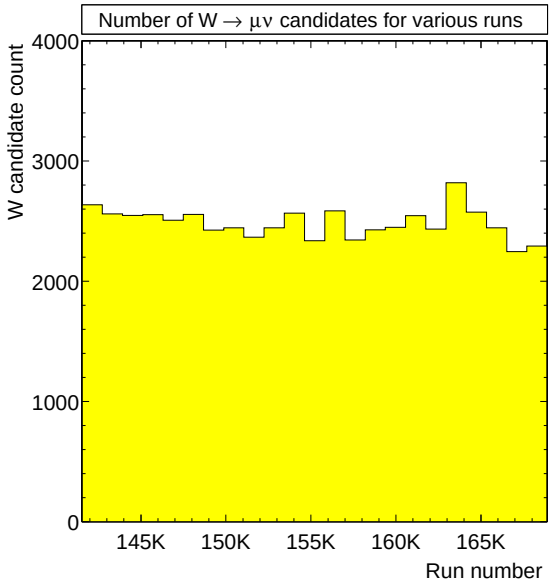

Figure 3: Number of W candidate events per a run range.

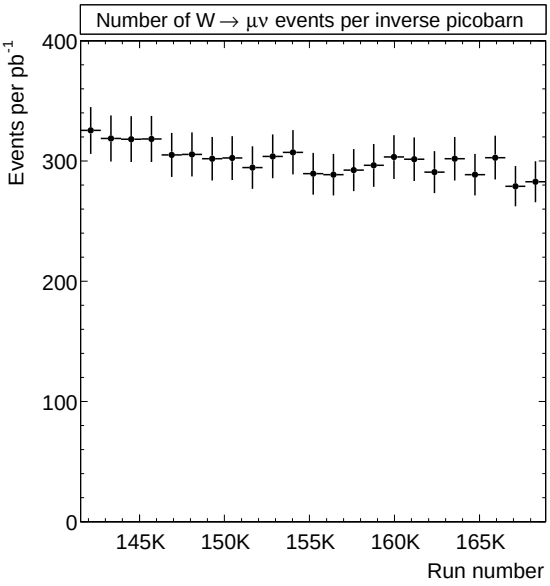

Figure 4: W candidate yield per inverse picobarn of delivered luminosity.

7 W Backgrounds

In this section we estimate the contribution of four main backgrounds to our $W \to \mu\nu$ candidate event sample. The backgrounds to be estimated are $Z \to \mu^+\mu^-$, $W \to \tau\nu$, QCD processes and cosmic rays. The sum of all these contributing background processes, described in detail in the subsections below, yields a total fraction of background events in the W sample of

$$b_W = 9.49 \pm 0.45\ \%. \tag{8}$$

7.1 Electroweak Processes

As it was already mentioned in Section 6 that $Z \to \mu\mu$ process can contribute to the sample of W candidates. In cases when a hard photon is radiated along the second muon or when the second track is not found the Z veto fails to filter out $Z \to \mu\mu$ decays.

$W \to \tau\nu$ can contribute to the sample of W candidates when, for example, decay $\tau \to \mu\nu\bar{\nu}$ happens. In case when muon from tau decay has $P_T \geq 20$ GeV/c, the event will appear in our W sample, given that $\not\!\!E_T \geq 20$ GeV.

The size of these background processes is calculated using electroweak Monte Carlo samples. While it is possible to calculate them in a standalone way, our standard background technique is best suited to a procedure where the electroweak processes treated simultaneously with the QCD background, which will be described in detail in the next subsection. The fraction of these background events will be found to be:

$$b^W_{Z\to\mu\mu} = 5.85 \pm 0.11\ \% \quad \text{and} \quad b^W_{W\to\tau\nu} = 3.10 \pm 0.12\ \%. \tag{9}$$

7.2 QCD Backgrounds

We will show in the next subsection that contribution from the cosmic rays is negligible, therefore we attribute the remainder of the background to the QCD processes.

Contrary to electroweak processes, the majority of QCD background events have relatively small missing transverse energy and large isolation ratio. For that reason we choose to look at the $\not\!\!E_T$ versus isolation ratio distributions to determine the number of the background events. Figures 5, 6 show these distributions for W candidates and $W \to \mu\nu$ simulation respectively, where the analysis cuts define four regions:

$$\mathbf{B}: \not\!\!E_T < 20\ GeV,\ Iso \geq 0.1 \qquad \mathbf{C}: \not\!\!E_T \geq 20\ GeV, Iso \geq 0.1$$
$$\mathbf{A}: \not\!\!E_T < 20\ GeV,\ Iso < 0.1 \qquad \mathbf{D}: \not\!\!E_T \geq 20\ GeV, Iso < 0.1$$

We will extract the QCD background in the signal region D by fitting data distri-

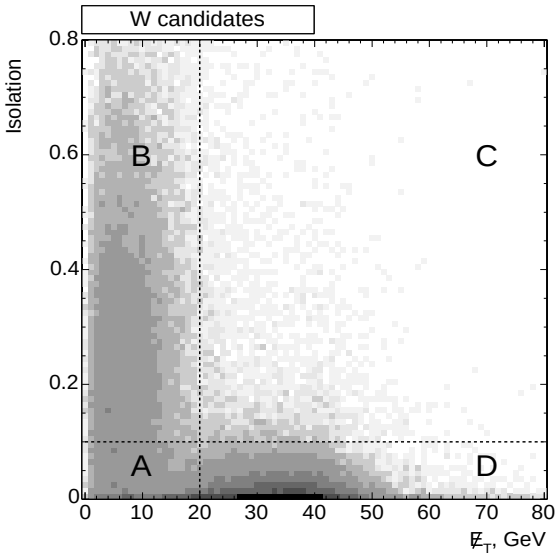

Figure 5: Isolation vs. $\not\!\!E_T$ distribution for W candidate events.

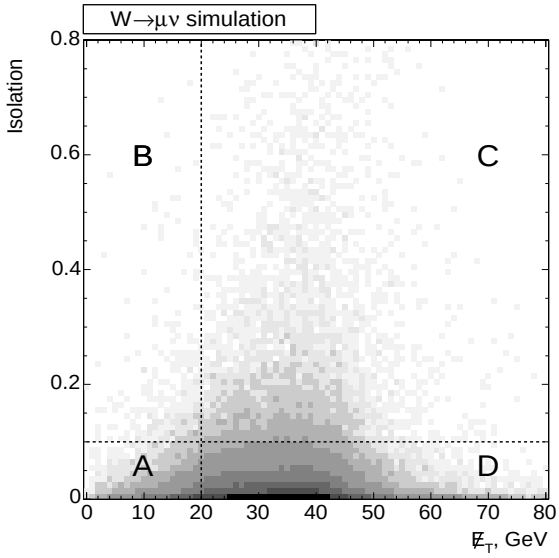

Figure 6: Isolation vs. $\not\!\!E_T$ distribution for $W \to \mu\nu$ simulation.

bution on figure 5 with the simulation shapes for electroweak processes and with the QCD shape obtained from the data distribution itself. Table 3 summarizes the event distributions for regions A, B, C, and D for W candidates and simulated electroweak processes.

Process Type	Generated	Number of Events			
	G	A	B	C	D
$W \to \mu\nu$	2,026,500	12,310	426	6,686	182,831
$Z \to \mu\mu$	472,500	5,372	192	1,143	29,428
$W \to \tau\nu$	490,000	478	12	50	1,512
W candidates	—	13,403	28,647	2,940	57,109
QCD	—	8,750	28,491	860	264

Table 3: Event distribution for regions A, B, C, and D for various processes.

In order to obtain the number of QCD events, we assume that for QCD background, the $\not{E}_T$ distribution does not depend on isolation ratio. In this case the number of QCD events $A_{QCD},\ B_{QCD},\ C_{QCD},\ D_{QCD}$ in the regions A, B, C, D can be expressed as:

$$\frac{A_{QCD}}{B_{QCD}} = \frac{D_{QCD}}{C_{QCD}} \quad \text{or} \quad \frac{A - A_{EWK}}{B - B_{EWK}} = \frac{D - D_{EWK}}{C - C_{EWK}}, \tag{10}$$

where $A,\ B,\ C,\ D$—the number of W candidate events in the regions A, B, C, D respectively. Similarly $A_{EWK},\ B_{EWK},\ C_{EWK},\ D_{EWK}$ is the number of $W \to \mu\nu$, $Z \to \mu\mu,\ W \to \tau\nu$ events in the regions A, B, C, D respectively.

We can perform the following substitution:

$$A_{EWK} = a \cdot W,\ B_{EWK} = b \cdot W,\ C_{EWK} = c \cdot W,\ D_{EWK} = d \cdot W, \tag{11}$$

where W—the number of expected $W \to \mu\nu$ events in the region D, and $a,\ b,\ c,\ d$—the coefficients that can be determined using the simulation sample numbers A, B, C, D, and G from Table 3. In order to calculate these coefficients we use the lepton universality for W decay $g \equiv \Gamma(W \to \tau\nu)/\Gamma(W \to \ell\nu) = 1.00$ [5] and the Standard Model prediction for the W and Z cross section ratio $R = 10.69$ from Equation 65:

$$a = \frac{A_{W\to\mu\nu}/G_{W\to\mu\nu} + A_{Z\to\mu\mu}/(R \cdot G_{Z\to\mu\mu}) + g \cdot A_{W\to\tau\nu}/G_{W\to\tau\nu}}{D_{W\to\mu\nu}/G_{W\to\mu\nu}} = 0.090\ , \tag{12}$$

$$b = \frac{B_{W\to\mu\nu}/G_{W\to\mu\nu} + B_{Z\to\mu\mu}/(R \cdot G_{Z\to\mu\mu}) + g \cdot B_{W\to\tau\nu}/G_{W\to\tau\nu}}{D_{W\to\mu\nu}/G_{W\to\mu\nu}} = 0.003\ , \tag{13}$$

$$c = \frac{C_{W\to\mu\nu}/G_{W\to\mu\nu} + C_{Z\to\mu\mu}/(R \cdot G_{Z\to\mu\mu}) + g \cdot C_{W\to\tau\nu}/G_{W\to\tau\nu}}{D_{W\to\mu\nu}/G_{W\to\mu\nu}} = 0.040\ , \tag{14}$$

$$d = \frac{D_{W\to\mu\nu}/G_{W\to\mu\nu} + D_{Z\to\mu\mu}/(R \cdot G_{Z\to\mu\mu}) + g \cdot D_{W\to\tau\nu}/G_{W\to\tau\nu}}{D_{W\to\mu\nu}/G_{W\to\mu\nu}} = 1.099\ . \tag{15}$$

We use substitution 11 in the expression 10 to obtain a quadratic equation

$$(A - a \cdot W)(C - c \cdot W) = (B - b \cdot W)(D - d \cdot W) \tag{16}$$

that has a valid root

$$W = \frac{-\beta + \sqrt{\beta^2 + 4\alpha\gamma}}{2\alpha}, \tag{17}$$

where $\alpha = (ac - bd),\ \beta = (b \cdot D + d \cdot B - a \cdot C - c \cdot A),\ \gamma = (A \cdot C - B \cdot D)$.

The calculated numbers for various processes contributing to the signal region D are:

$$N_W = 51,734 \pm 257 \tag{18}$$

$$B^W_{Z\to\mu\mu} = 3,341 \pm 61 \quad B^W_{W\to\tau\nu} = 1,769 \pm 67 \quad B^W_{QCD} = 264 \pm 83 \tag{19}$$

where the systematic error includes both the uncertainties on parameters g, R and the uncertainty of our assumption that in QCD events $\not\!\!E_T$ and isolation variables are independent. In order to test this assumption we study the variation in the number of background events when isolation or $\not\!\!E_T$ cuts are changing. When we vary the $\not\!\!E_T$ cut we fix the regions C and D but we let the regions A and B change. Likewise, when we change the isolation ratio cut we fix the regions A and D but we let the regions B and C vary. Figures 7 and 8 shows the dependence of the calculated backgrounds on $\not\!\!E_T$ and isolation ratio values respectively.

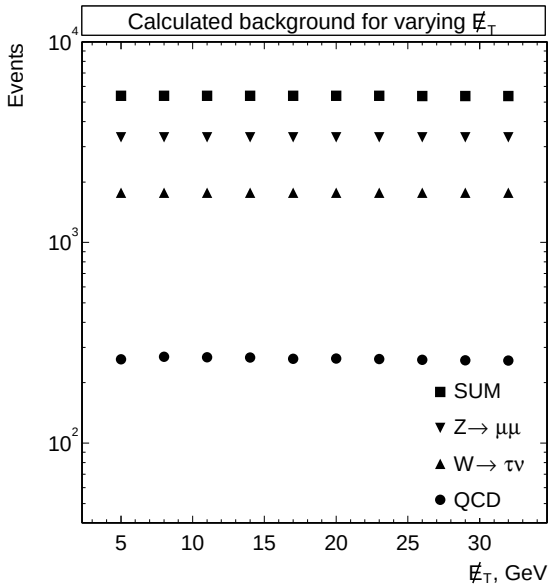

Figure 7: The background dependence on $\not\!\!E_T$ cut for W candidates.

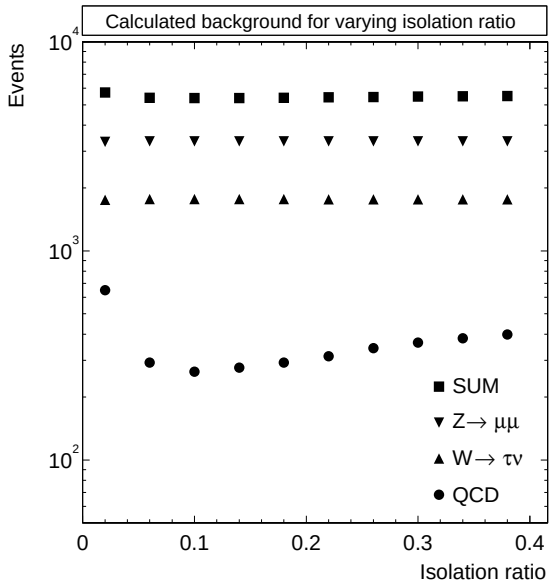

Figure 8: The background dependence on isolation ratio cut for W candidates.

As listed in Tables 4 and 5 the variation of cuts affects largely the calculation of QCD background. Therefore our estimate of the systematic uncertainty on the QCD

$\not{E}_T$ cut	QCD	$W \to \tau\nu$	$Z \to \mu\mu$	background sum
5 GeV	261	1,769	3,347	5,378
8 GeV	270	1,769	3,346	5,385
11 GeV	268	1,769	3,347	5,384
14 GeV	267	1,769	3,347	5,383
17 GeV	263	1,769	3,347	5,379
20 GeV	264	1,769	3,347	5,380
23 GeV	262	1,769	3,347	5,378
26 GeV	260	1,769	3,347	5,376
29 GeV	258	1,769	3,347	5,375
32 GeV	258	1,769	3,347	5,375

Table 4: The calculated number of the background events in the signal region D for varying $\not{E}_T$ cut.

isolation ratio cut	QCD	$W \to \tau\nu$	$Z \to \mu\mu$	background sum
0.02	649	1,757	3,324	5,731
0.06	293	1,768	3,345	5,406
0.10	264	1,769	3,348	5,380
0.14	277	1,769	3,346	5,391
0.18	292	1,768	3,345	5,406
0.22	313	1,768	3,344	5,425
0.26	342	1,767	3,342	5,452
0.30	364	1,766	3,341	5,471
0.34	382	1,766	3,340	5,487
0.38	399	1,765	3,339	5,503

Table 5: The calculated number of the background events in the signal region D for varying isolation ratio cut.

background is obtained by varying the interval of the isolation variable from 0.1 to 0.4. Therefore, our estimate of systematic uncertainty on QCD background comes from the result variation in the interval of isolation variable from 0.1 to 0.4. Half of this variation is taken as our systematic error when evaluating the relative fraction of QCD background events

$$b^W_{QCD} = 0.46 \pm 0.12\ \%. \tag{20}$$

The uncertainty on calculation of $Z \to \mu\mu$ background shown in 19 comes from the 1.9 % uncertainty of the recent R measurement [14]. The uncertainty associated with $W \to \tau\nu$ background quoted in 19 comes from the 2.9 % uncertainty on the lepton universality measurements [5]. The relative fraction of electroweak background events

is given in Equation 9.

Figure 9 plots the distributions of the $\not\!\!E_T$ variable and shows the calculated relative contributions of signal and background events. The shapes of the $W \to \mu\nu$ signal, $W \to \tau\nu$ background, and $Z \to \mu^+\mu^-$ background contributions are taken directly from simulation. The shape of the QCD background is obtained from the data using events that have an isolation ratio greater than 0.1 but pass all other analysis cuts. We note that our method relies on the assumption that $\not\!\!E_T$ shape for the QCD background from high isolation region models that from low isolation region. The good fit in this plot verifies that this assumption is robust.

7.3 Cosmic Background

As it was specified in Section 5 the signature of W event can be imitated by a cosmic ray when only one leg of the cosmic is reconstructed. Such an event may pass both Z veto and $\not\!\!E_T$ cut due to the transverse momentum imbalance. In this section we attempt to determine the fraction of events due to cosmic rays, that slipped through cosmic tagger. To study such events, we prepare a "cosmic-rich" data sample: muons must pass the requirements of Table 1, except for the impact parameter cut, and in addition only events with the small number of tracks $n_{trk} < 5$ are selected. Our "cosmic-rich" sample contains 178 events out of which 119 events have both CMP and CMU hits on the opposite side of the detector from the trigger muon. We conclude that about $119/178 = 67 \pm 4$ % of cosmic events will opposite side muon hits.

For cosmic ray event the muon chamber hits are positioned near the straight line of a cosmic ray trajectory. We search for both CMP and CMU hits which are positioned on the opposite side of the detector from the trigger muon according to the following rules:

- Look for a CMP hit, which is the closest to the extrapolated cosmic ray track and calculate the azimuthal location in the CDF coordinate system. If the distance between found hit and expected cosmic ray is small: $|\phi_{CMP} - \phi_{cosm}| \geq 0.5$ rad, consider the event.

- Look for CMU hits matching the found CMP hit and calculate the azimuthal location. If the distance between found CMU and CMP hits is small: $|\phi_{CMP} - \phi_{CMU}| \geq 0.05$ rad, consider the event.

Using this algorithm we found 398 events out of the W candidate sample. Some of these are cosmic ray events that passed the cosmic tagger as discussed above. However there are additional Z events that escaped Z -veto perhaps because of hard photon radiation along the muon, and W events with jets and noise.

To understand the true cosmic fraction, we can examine the CMU hit position distribution relative to the projected cosmic ray hit both in transverse plane and along $\hat{z}$ direction. In transverse plane collision events from W with jet or Z decay may have CMU hits on the opposite side of the detector from the trigger muon. However, we do

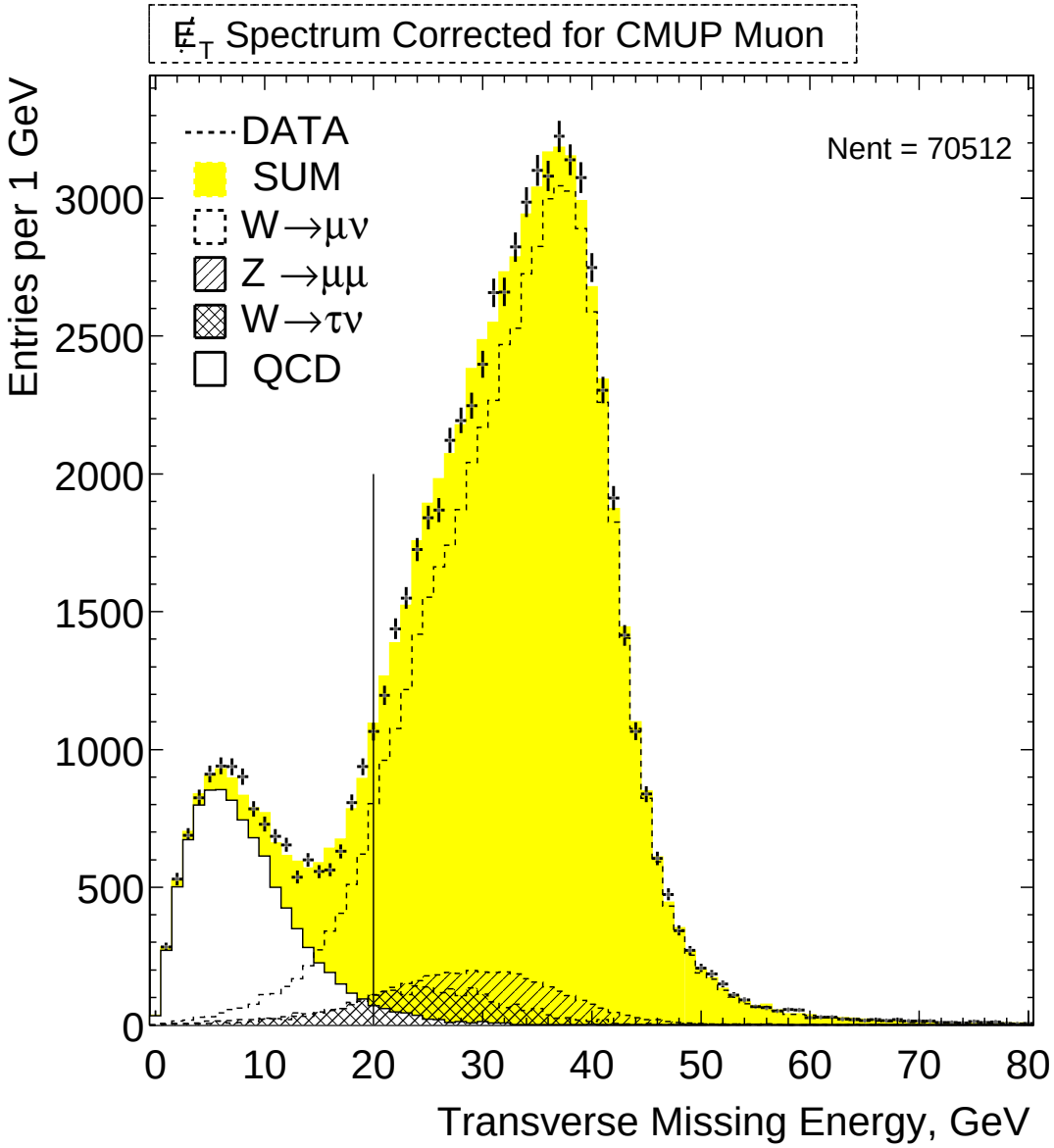

Figure 9: $\not\!\!E_T$ in data and Monte Carlo for $W \rightarrow \mu\nu$ candidate events.

not expect "back-to-back" signature for the collision events in $\hat{z}$ direction. Figures 10 and 11 show $z_{CMU} - z_{cosm}$ variable distribution both for "cosmic-rich" and W candidate samples. The distribution for cosmic sample peaks near 0 with the gaussian width around 40 cm, whereas the distribution for W sample looks rather flat with characteristic width of 170 cm. To determine the number of possible cosmic events in W data we fit the Figure 11 distribution with the sum of wide and narrow gaussian dsitributions representing collision and potential cosmic events respectively. The means of these distributions are fixed at 0. The fit sets the amplitude of cosmic background at it's

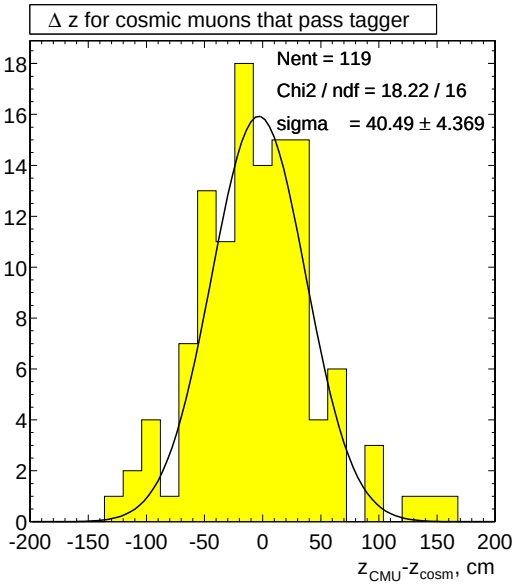

Figure 10: The difference between $\hat{z}$ components of CMU hits and projected cosmic ray hit for cosmics data.

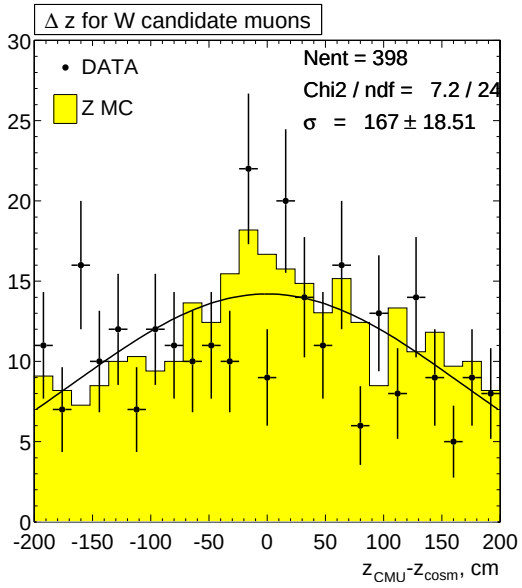

Figure 11: The difference between $\hat{z}$ components of CMU hits and projected cosmic ray hit for W data.

lowest boundary equal to 0 events. Based on the number of the data events in the range of $-40 < z_{CMU} - z_{cosm} < 40$ cm we establish an upper limit on the number of cosmic events. We count 75 events, which for the 95 % confidence level result in the upper limit of 17.3. For the total number of cosmic events we divide this number by the fraction of cosmic rays with the opposite side hits found both in CMU and CMP:

$$B^W_{cosm} = \frac{0.00 \pm^{17.3}_{0.00}}{0.67 \pm 0.04} = 0.00 \pm^{25.85}_{0.00} \quad \text{or} \quad b^W_{cosm} = 0.00 \pm^{0.04}_{0.00} \ \%. \tag{21}$$

8 Z Selection Criteria

The $Z \to \mu^+\mu^-$ cross section measurement utilizes the same high-P_T muon dataset and the same good run list that are used for the W measurement, which is described in detail in sections 2 and 4.

Every Z candidate event represents a muon-track pair, in which both legs must pass a loose set of cuts and at least one leg must pass a tight selection. This way we can greatly improve our acceptance and simplify our efficiency calculation without taking on additional background.

Figure 12 shows the invariant mass distribution for the selected $Z \to \mu^+\mu^-$ candidate events. The measured muon P_T in simulation events has been tuned to give the best agreement with the data [4].

The tight muon is required to pass all of the kinematic and identification criteria used to select muon candidates in the W analysis. The full set of selection criteria for

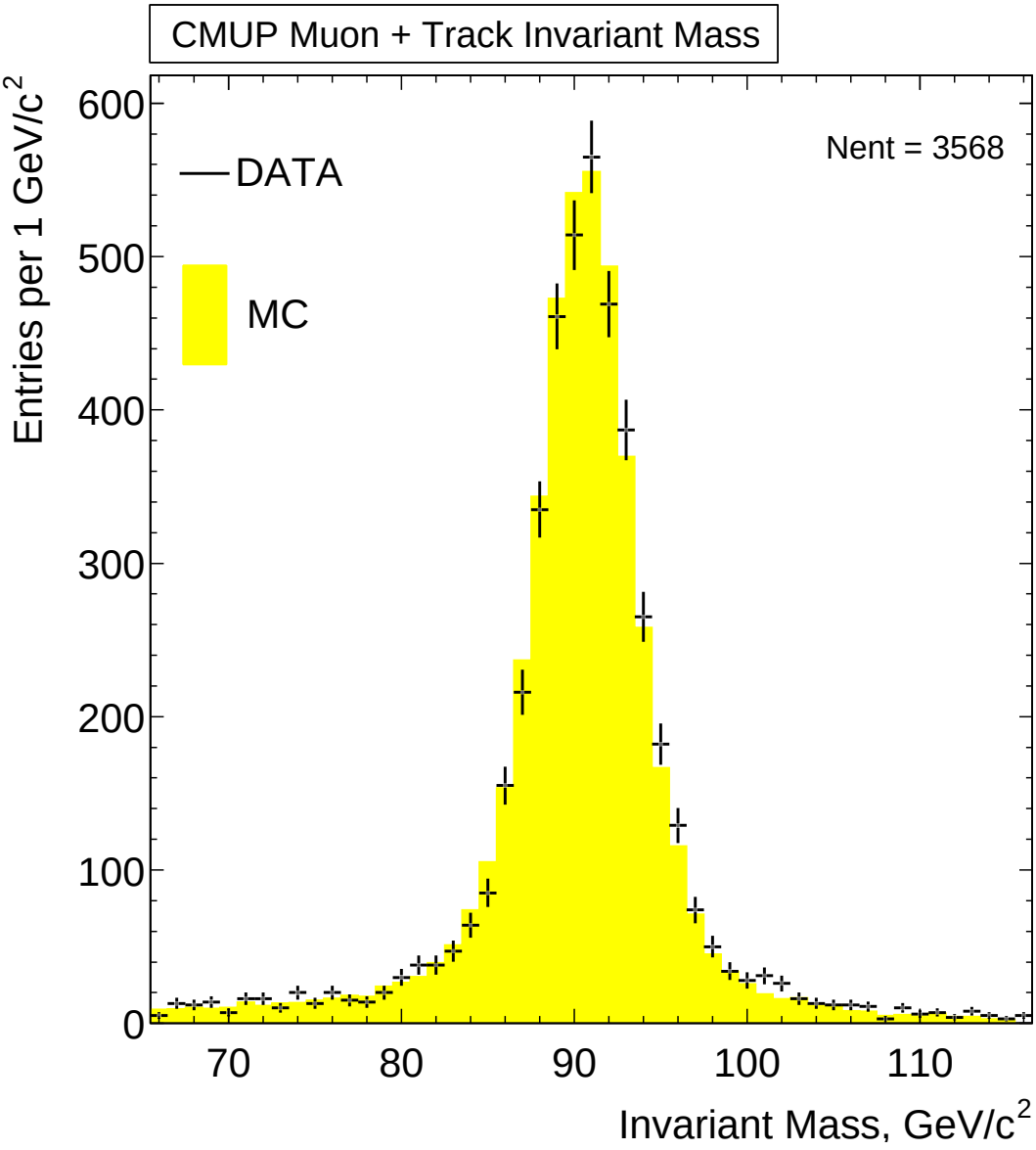

Figure 12: Dimuon invariant mass $M_{\mu\mu}$ distribution in data and simulation for $Z \rightarrow \mu^+\mu^-$ candidate events.

the tight muon was shown in Table 1. Note that the tight muon is also required to be the trigger muon in the event. This trigger requirement means that we reject events that make it into our sample exclusively via the CMX high-P_T trigger path even if the events contain a second CMUP muon candidate that satisfies all of the other selection criteria for loose muons.

Loose muons are isolated COT tracks pointing at minimum ionizing energy deposits

in the calorimeter. We also make sure that the loose muon leg traverse all eight COT super-layers before exiting the tracker. This requirement guarantees high uniform efficiency for COT track reconstruction.

The full set of kinematic and identification cuts applied to the loose muon are listed in upper part of Table 6.

Requirement	Purpose	Number of Passed Events
Inclusive Muon	Quality Muon	77,140
Second High-P_TTrack	Second Leg of Z	9,565
$P_T > 20$ GeV/c	Low-P_TNoise Reduction	6,202
$\lvert z_0^T - z_0^L \rvert < 4$ cm	Same Vertex Tracks	6,084
COT Radius $\rho \geq 140$ cm	Fiducial Tracks	4,408
$E_{EM} < 2$ GeV	Minimum Ionizing Deposition	4,223
$E_{HAD} < 6$ GeV	Minimum Ionizing Deposition	4,186
$3 \leq N_{Seg}^{Ax}$, $3 \leq N_{Seg}^{St}$	Good Track Quality	4,047
$\lvert d_0^{cor} \rvert < 0.2$ cm	Good Track Quality	4,018
$\chi^2_{COT}/ndf < 2$	Good Track Quality	4,018
$Iso < 0.1$	Background Reduction	3,905
$66 < M < 166$ GeV/c^2	Mass Range of Measurement	3,568
$Q^T = -Q^L$	Opposite Charge Tracks	3,568

Table 6: Loose muon cuts for $Z \rightarrow \mu^+\mu^-$ selection.

In order to ensure that both muons come from the same event vertex, we require that the distance between z_0 of the two tracks is less than 4.0 cm. We also require that the two muon candidates have opposite charges. For the current data set, neither of these requirements removes any events from our candidate sample. As in other CDF electroweak analyses [15] we require that the invariant mass of the muon pair lies between 66 GeV/$c^2$and 116 GeV/c^2.

In some fraction of candidate events, we find two reconstructed muons that satisfy the tight muon selection criteria. Since the loose muon criteria are a subset of the tight muon criteria, all events of this type make it into our final candidate sample. However, in calculating the overall efficiency for selecting $Z \rightarrow \mu^+\mu^-$ events, we must consider events with two muons pointing at both the CMU and CMP chambers as a special case since both will have the opportunity to satisfy the tight muon requirements and the trigger. This calculation will be discussed in much greater detail in a Section 11.2 of this note.

The yield of Z candidate events per data-taking runs for the whole period is shown on Figure 13. The run interval is sampled in the ranges, with the corresponding integrated luminosity of at least 8 pb^{-1}. Figure 14 shows Z event count per inverse picobarn of delivered luminosity for various run ranges, which is a relatively flat distribution.

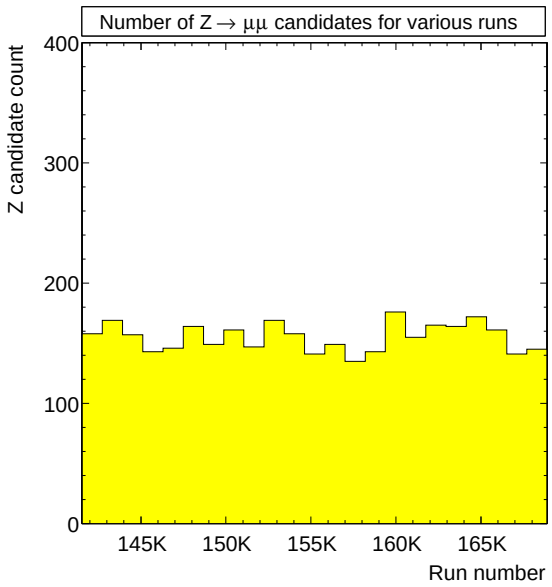

Figure 13: Number of Z candidate events per a run range.

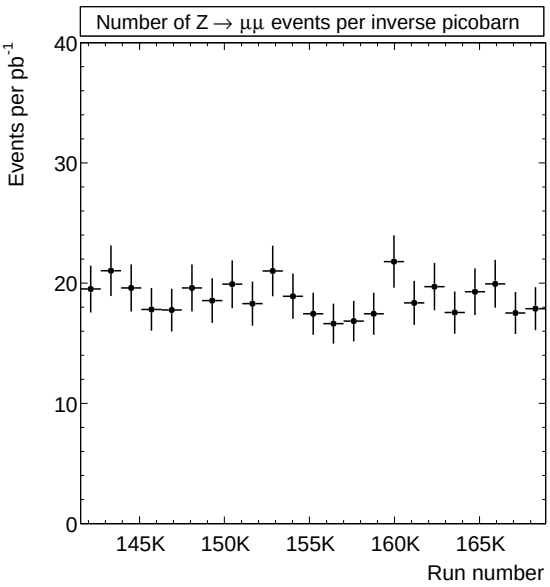

Figure 14: Z candidate yield per inverse picobarn of delivered luminosity.

9 Z Backgrounds

Because of the requirement for a second muon we expect the fraction of background events for $Z \to \mu^+\mu^-$ process to be much smaller than in case of $W \to \mu\nu$ analysis. The leading backgrounds described in this section are cosmic rays, $Z \to \tau^+\tau^-$ and QCD processes. The sum of all these contributing background processes, described in detail in the subsections below, yields a total fraction of background events in the Z sample of

$$b_Z = 0.36 \pm 0.19\ \%. \tag{22}$$

9.1 Cosmic Background

The cosmic ray background is estimated by looking at the 3-D opening angle between muon legs in Z decay. We expect muon legs from cosmic rays to be "back-to-back" with the opening angle distribution peaking at π as shown on figure 15. This distribution falls sharply and ends at the angle value of about 2.8 radians. We compare opening angle distributions in Z data versus $Z \to \mu\mu$ simulation as shown in figure 16. We find 2207 data and 19572 simulation events in the angle interval from 0 to 2.8 radians. The total number of events is 3568 for data Z candidates and 31556 for simulation. We normalize the distributions such that the areas for both Z data and simulation histograms are equal in the interval from 0 to 2.8 radians. The normalization scale factor is:

$$19572/(31556 - 19572) = 0.612 \pm 0.003\ . \tag{23}$$

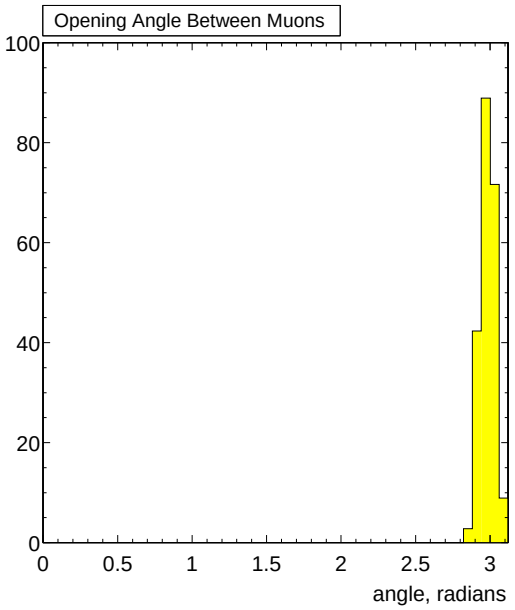

Figure 15: The distribution of 3-D opening angle between muon legs in cosmic ray events.

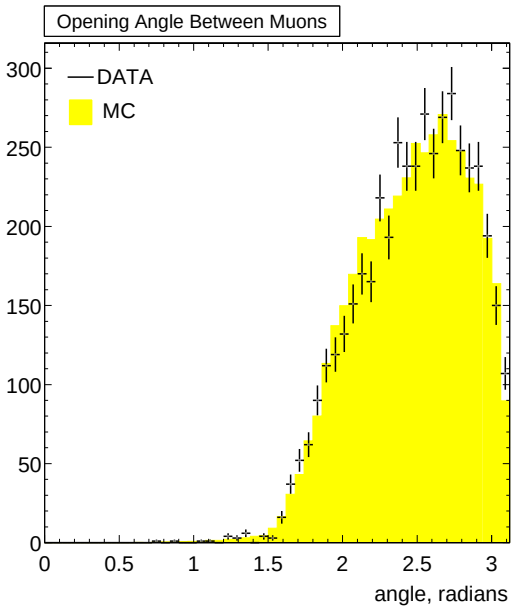

Figure 16: The distribution of 3-D opening angle between muon legs in collision data, compared to $Z \to \mu\mu$ Monte Carlo.

We then look at the excess of the entries in the data over the simulation in the region from 2.8 to π radians. The estimated fraction of cosmic is

$$B^Z_{cosm} = (3568 - 2207) - 2207 \cdot 0.612 = 10 \pm 7 \quad \text{or} \quad b^Z_{cosm} = 0.27 \pm 0.19\ \%. \quad (24)$$

9.2 Electroweak Processes

The background from $Z \to \tau\tau$ process is significantly suppressed both by kinematics and by the square of branching ratio $B(\tau \to \mu\nu\bar{\nu})$. Kinematic suppression is due to the partial smearing of di-muon invariant mass distribution toward lower values outside the $66 - 116$ GeV/c^2 mass window. Using the 490,000 simulated $Z \to \tau\tau$ events we counted 27 events. On the other hand, out of 472,500 simulated $Z \to \mu\mu$ events, we select 31,556 events. The estimated fraction of background event due to $Z \to \tau\tau$ process is, therefore

$$b^Z_{\tau\tau} = \frac{27/490,000}{31,556/472,500} = 0.089 \pm 0.017\ \%, \quad (25)$$

where the uncertainty is due to the limited statistics.

9.3 QCD Backgrounds

We attribute the remainder of the contributing background to the QCD processes. Contrary to cosmic rays and electroweak processes, the di-muon fakes from these back-

ground events may have the same sign charges. In order to estimate the number of the QCD background events we assume that the number of fake events where both tracks have the same charges should be close to the number of fake events where both tracks have the opposite charges. For the current data set, we observe no same charge events and our estimate of of the number of QCD events is

$$B^{Z}_{QCD} = 0^{+1.1}_{-0} \quad \text{or} \quad b_Z = 0.00^{+0.03}_{-0.00}\ \%, \tag{26}$$

where the error intervals come from 68% confidence level for Poisson statistics with 0 counted events.

10 Acceptances

The geometrical and kinematic requirements of W and Z selections result in limited acceptance for detecting these processes. To calculate the acceptance for W and Z cases we use the Monte Carlo simulation samples wewk0m and zewk0m. Tables 7 and 8 summarize the number of events that pass various geometrical and kinematic cuts.

Selection Stage	Number of Events
All Simulated Events	2,026,500
Luminous Beam Region $\lvert z_0\rvert < 60\ cm$	1,960,283
CMUP Fiducial Track	365,891
COT Radius $\rho \geq 140\ cm$	365,891
Track $P_T \geq 20$ GeV/c	304,999
$\not\!\!E_T \geq 20$ GeV	285,151
Z -veto	284,428

Table 7: W acceptance calculation.

Selection Stage	Number of Events
All Simulated Events	472,500
Beam Region $\lvert z_0\rvert < 60\ cm$	456,912
$66 < M_{gen} < 116$ GeV/c^2	341,119
First Leg CMUP Fiducial	113,582
First Leg $P_T \geq 20$ GeV/c	103,212
Second Leg $\rho \geq 140\ cm$	39,541
Second Leg $P_T \geq 20$ GeV/c	39,455
$66 < M_{rec} < 116$ GeV/c^2	39,341

Table 8: Z acceptance calculation.

The values above the double line in these tables are the number of events that represent denominator in the ratio for the acceptance calculation. The number of events in numerator are taken from the last entry of the Tables 7, 8. Thus:

$$A_W = 284,428/1,960,283 = 0.1451^{+0.0020}_{-0.0024} \tag{27}$$

$$A_Z = 39,341/341,119 = 0.1153^{+0.0021}_{-0.0026} \tag{28}$$

where A_W — is the acceptance for selecting $W \to \mu\nu$ process, and A_Z — is the acceptance for selecting $Z \to \mu\mu$ process. The expected ratio of acceptances is

$$A_Z/A_W = 0.1153/0.1451 = 0.7949^{+0.0068}_{-0.0076} \tag{29}$$

The errors quoted in Equations 27, 28 and 29 are the combined systematic uncertainties that have been studied previously in greater detail in [4]. The uncertainties in

acceptance due to the parton distribution in colliding protons and anti-protons was studied thoroughly in [16]. The results of these studies are summarized in the Table 9.

Uncertainty Source	δA_W, %	δA_Z, %	$\delta(A_Z/A_W)$, %
Simulation Statistics	0.18	0.46	0.49
Momentum Scale	0.21	0.05	0.16
Recoil Model	0.36	—	0.36
W Z Transverse Motion	0.04	0.08	0.12
Parton Distributions	+1.30 -1.61	+1.74 -2.23	+0.56 -0.71
All Combined	+1.38 -1.67	+1.80 -2.28	+0.85 -0.96

Table 9: Summary of uncertainties for calculating the acceptance ratio

The leading source of systematic error is the uncertainty on parton distribution functions with relative error of about 2 % for W and Z acceptances. However, for the ratio of acceptances this uncertainty is signigicantly reduced to the relative error value of about 0.7 %.

Finally a parameter which we will need for evaluating the efficiency of Z selection cuts in Section 11 is the fraction of events where both muon legs from Z decay fall into the fiducial region of both CMU and CMP chambers. Out of 39,341 selected events passing basic kinematic and geometrical requirements from Table 8 we find 10,307 events with both legs of Z pointing to CMU and CMP fiducial regions:

$$f = 10,307/39,341 = 0.262 \pm 0.002 \tag{30}$$

where the error is based on statistical uncertainty only.

11 Efficiencies

Three major types of the muon efficiencies correspond to muon reconstruction, triggering, and identification. In order to account for potential variation of these efficiencies during the data-taking period we determine them directly from our Z candidate event sample. The muons from Z decay will have a similar kinematics to those from W decay and will be embedded in a similar event environment.

The method for measuring the efficiencies of various requirements that we apply for muon is based on utilizing the unbiased leg of Z boson. The event sample in this case is merely two high-P_T tracks that have opposite sign charges and form an invariant mass within the window $80 < M < 100$ GeV/c^2. Regardless of what efficiency we measure, the biased leg must always be a reconstructed muon that triggered the event and passes all muon identification cuts. The unbiased or *probe* leg must at least point to fiducial regions of both CMU and CMP muon chambers.

To measure the reconstruction efficiency we apply muon identification cuts to the probe leg except for the stub matching requirements. We then divide the number of

probe legs that have both CMU and CMP stubs reconstructed by the number of all found probe legs:

$$\epsilon_{rec} = 2,499/2,735 = 0.9137 \pm 0.0054 \tag{31}$$

To measure the trigger efficiency we require the probe leg to have both CMU and CMP stubs reconstructed. We also apply all muon identification cuts to the unbiased leg including the stub matching requirements. We then take a ratio of the number of probe legs that have associated local trigger to the number of all found probe legs:

$$\epsilon_{trg} = 2,116/2,355 = 0.8985 \pm 0.0062 \ . \tag{32}$$

In addition to the local trigger, there are inefficiencies associated to the global trigger path. We found that out of 722 Z events for which at least one leg has associated local trigger, 720 events have passed the global trigger requirement:

$$\epsilon_{L3} = 720/722 = 0.9972 \pm 0.0020 \ . \tag{33}$$

To measure the efficiency of muon identification cuts we require the probe leg to have both CMU and CMP stubs reconstructed. We also apply remaining muon identification cuts that we are not measuring to the unbiased leg. The efficiencies for muon identification when various cuts are applied simultaneously are:

ϵ'_{id} — the efficiency to identify the loose leg,

ϵ_{dx} — the efficiency of matching muon to its CMU and CMP stubs,

ϵ_{id} — the efficiency to identify the tight leg.

The measured values for these parameters are listed as the last three entries in the Table 10 along with the other efficiencies.

Applied Cut	Label	Ratio	Efficiency
$E_{EM} < 2$ GeV	ϵ_{em}	2,355 / 2,428	0.9699±0.0035
$E_{HAD} < 6$ GeV	ϵ_{had}	2,355 / 2,394	0.9837±0.0026
$N_{Seg}^{Ax} \geq 3$, $N_{Seg}^{St} \geq 3$	ϵ_{seg}	2,355 / 2,419	0.9735±0.0033
$\lvert d_0^{cor}\rvert < 0.2\ cm$	ϵ_{d_0}	2,355 / 2,361	0.9975±0.0010
$\chi^2_{COT}/ndf < 2$	ϵ_{χ}	2,355 / 2,355	1.000
$Iso < 0.1$	ϵ_{iso}	2,355 / 2,395	0.9833±0.0026
All Combined Without Muon Stub Matching	ϵ'_{id}	2,355 / 2,595	0.9075±0.0057
$\lvert\Delta X\rvert_{CMU} < 3\ cm$ $\lvert\Delta X\rvert_{CMP} < 5\ cm$	ϵ_{dx}	2,355 / 2,499	0.9424±0.0047
All Combined	ϵ_{id}	2,355 / 2,748	0.8570±0.0067

Table 10: Muon identification efficiencies

11.1 Efficiency for Selecting W

We define the efficiency of detecting the muon from W decay according to the expression

$$\epsilon_W = \epsilon_{z_0}\, \epsilon_W^{cr}\, \epsilon_{trk}\, \epsilon_{L3}\, \epsilon_{trg}\, \epsilon_{rec}\, \epsilon_{id}. \tag{34}$$

The last four variables were described in the previous subsection. The additional efficiencies related to the W selection are:

ϵ_{z0} — the efficiency of z_0 track cut,

ϵ_W^{cr} — the overefficiency of cosmic ray tagger,

ϵ_{trk} — COT track reconstruction efficiency.

The efficiency of the z_0 track cut is measured independently by using minimum bias events. The method is based on the measurement of longitudinal profile of the $p\bar{p}$ luminous region and calculating the fraction of events that falls inside the region $|z_0| < 60\ cm$. A separate note [4] describes the measurement in more detail and quotes the efficiency value:

$$\epsilon_{z_0} = 0.948 \pm 0.003\ , \tag{35}$$

where statistical and systematic uncertainties have been included in the error.

A small fraction of muon tracks originating from W decay can be misidentified as a cosmic ray by the cosmic tagger. The overefficiency of cosmic ray tagger ϵ_{cr} is measured using the electron W and Z samples [8].Since the electron samples are free of cosmic ray background, the fake number of tags observed in these samples is a reliable measure of the overefficiency of our algorithm for tagging real $W \to \mu\nu$ and $Z \to \mu\mu$ processes. The method is outlined in more detail in a separate note [4]. The measured values are:

$$\epsilon_W^{cr} = 0.9999 \pm 0.0001 \quad \text{and} \quad \epsilon_Z^{cr} = 0.9994 \pm 0.0006\ , \tag{36}$$

where the quoted error includes both statistical and systematic uncertainties.

The tracking efficiency in muon data was measured using the Monte Carlo track embedding technique and documented in a separate note [17]. The quoted value for the absolute tracking efficiency is

$$\epsilon_{trk} = 0.996^{+0.004}_{-0.009}\ , \tag{37}$$

which is also applicable for high-P_T isolated muons. In order to account for the track reconstruction in calculating our acceptance numbers we have to evaluate tracking efficiency in Monte Carlo. We use $W \to \mu\nu$ simulation. Our efficiency denominator is 821967, which is the number of COT fiducial high-P_T HEPG muons from prompt W decay. Out of these muons 821752 have associated reconstructed tracks. The resulting efficiency number is $821752/821967 = 99.9738 \pm 0.0018$ %, which is 1.00 when rounded to the precision of our data measurement

We use the efficiency numbers from Table 10 and Equations 31–37 to calculate the efficiency for $W \to \mu\nu$ process:

$$\epsilon_W = 0.661^{+0.009}_{-0.010}\ . \tag{38}$$

11.2 Efficiency for Selecting Z

The efficiency expression for selecting $Z \to \mu^+\mu^-$ candidates differs significantly from efficiency of $W \to \mu\nu$, since our selection requires both tight and loose muons are present in our final sample.

We define the efficiency of detecting the loose muon according to the expression

$$\epsilon_L = \epsilon_{trk}\epsilon'_{id} \ , \tag{39}$$

where ϵ_{trk} — track reconstruction efficiency; ϵ'_{id} — the combined efficiency of muon identification cuts without applying stub matching requirements.

Detecting a tight muon requires CMU and CMP stub reconstruction and matching, and the efficiency can be expressed as

$$\epsilon_T = \epsilon_L\epsilon_{rec}\epsilon_{dx} \ , \tag{40}$$

where ϵ_{rec} - efficiency for a track to be linked to both CMU and CMP reconstructed stubs; and ϵ_{dx} - efficiency for a track to match both CMU and CMP stubs within ΔX cuts.

To combine ϵ_L and ϵ_T into ϵ_Z, we must consider several distinct categories of muon pairs:

- *Both muons are in CMUP fiducial region with CMU and CMP stubs.*

  When both CMU and CMP stubs are present for loose muon the efficiency ϵ_L is multiplied by the factor ϵ_{rec}. Also, depending on track-stub matching, the loose muon efficiency becomes

  $$\epsilon_L\epsilon_{rec}(1-\epsilon_{dx}) \tag{41}$$

  when muon fails ΔX cuts, and

  $$\epsilon_L\epsilon_{rec}\epsilon_{dx} = \epsilon_T \tag{42}$$

  when muon passes ΔX cuts. The efficiency combinations for various cases are:

ϵ_T^2	–	both muons pass tight selection
$\epsilon_T\epsilon_L\epsilon_{rec}(1-\epsilon_{dx})$	–	only first muon passes tight selection
$\epsilon_L\epsilon_{rec}(1-\epsilon_{dx})\epsilon_T$	–	only second muon passes tight selection
$(\epsilon_L\epsilon_{rec}(1-\epsilon_{dx}))^2$	–	no tight muon - event is rejected

  We also have to take care of trigger efficiencies for each case considered above:

$\epsilon_{trg}(2-\epsilon_{trg})$	–	both muons pass tight selection and at least one muon triggers the event
ϵ_{trg}	–	first muon is tight and triggers the event
ϵ_{trg}	–	second muon is tight and triggers the event

By combining the efficiencies for each cases we obtain the following result for this category of $Z \to \mu^+\mu^-$ events:

$$\epsilon_{trg}(2-\epsilon_{trg})\epsilon_T^2 + 2\epsilon_{trg}\epsilon_T\epsilon_L\epsilon_{rec}(1-\epsilon_{dx}) = \epsilon_{trg}\epsilon_T\epsilon_L\epsilon_{rec}(2-\epsilon_{trg}\epsilon_{dx}). \tag{43}$$

- *Both legs in CMUP region but only the tight muon has both CMU and CMP stubs.*

  In this case, for some reason the muon reconstruction fails to provide both CMU and CMP stubs for loose leg of Z. Under this condition the efficiency for the loose leg becomes

  $$\epsilon_L(1-\epsilon_{rec}). \tag{44}$$

  The only observed outcomes in this case is when first leg is tight and second is loose or first leg is loose and second is tight, the sum over which is

  $$2\epsilon_T\epsilon_L(1-\epsilon_{rec}). \tag{45}$$

  The trigger efficiency enters the ϵ_Z expression for this case simply as a factor ϵ_{trg}, since only the tight muon can trigger the event.

  The combined ϵ_Z result for this category of $Z \to \mu^+\mu^-$ events is

  $$2\epsilon_{trg}\epsilon_T\epsilon_L(1-\epsilon_{rec}). \tag{46}$$

- *Only tight muon is CMUP-fiducial, but loose leg is outside of CMUP region.*

  For this case, the loose leg of Z is directed in such a way that it does not hit both CMU and CMP chambers at the same time. Under this condition, the efficiency to detect the loose leg is simply ϵ_L. The only one observed outcome in this case is when CMUP leg is tight and the other leg is loose, which corresponds to the selection efficiency

  $$\epsilon_T\epsilon_L. \tag{47}$$

  The trigger efficiency enters the ϵ_Z expression for this case simply as a factor ϵ_{trg}, since only the tight muon can trigger the event.

  The combined ϵ_Z result for this category of $Z \to \mu^+\mu^-$ events becomes

  $$\epsilon_{trg}\epsilon_T\epsilon_L. \tag{48}$$

Now that we have considered all the cases, we can combine them together weighing by the fractions[2] f and $(1-f)$ for Equations 43–46 and 48 respectively:

$$f\epsilon_{trg}\epsilon_T\epsilon_L\epsilon_{rec}(2-\epsilon_{trg}\epsilon_{dx}) + 2f\epsilon_{trg}\epsilon_T\epsilon_L(1-\epsilon_{rec}) + (1-f)\epsilon_{trg}\epsilon_T\epsilon_L =$$

$$= \epsilon_{trg}\epsilon_T\epsilon_L[1+f(1-\epsilon_{trg}\epsilon_{rec}\epsilon_{dx})] \tag{49}$$

[2]refer to section 10 for definition of f

To finalize our result we multiply the combined result 49 by the efficiencies of track z_0, cosmic tagging and global trigger:

$$\epsilon_Z = \epsilon_{z0}\epsilon_Z^{cr}\epsilon_{L3}\epsilon_{trg}\epsilon_T\epsilon_L[1 + f(1 - \epsilon_{trg}\epsilon_{rec}\epsilon_{dx})]. \tag{50}$$

While expression for ϵ_Z looks a bit complicated we note that when $\epsilon_{trg} \approx 1$, $\epsilon_{rec} \approx 1$, and $\epsilon_{dx} \approx 1$ the expression $[1+f(1-\epsilon_{trg}\epsilon_{rec}\epsilon_{dx})]$ in brackets reduces to ≈ 1 for arbitrary values of f. Thus, Equation 50 turns into more simplified form $\epsilon_{z0}\epsilon_Z^{cr}\epsilon_{L3}\epsilon_{trg}\epsilon_T\epsilon_L$, which is a good estimate for ϵ_Z.

We use the efficiency numbers from Equations 31, 32, 33 and Table 10 to calculate the efficiency for $Z \to \mu^+\mu^-$ process:

$$\epsilon_Z = 0.633^{+0.011}_{-0.015} \tag{51}$$

11.3 Ratio of Efficiencies

To calculate the ratio of efficiencies ϵ_Z/ϵ_W we use the Equations 34 and 50. When we evaluate this ratio we notice that the product of efficiencies $\epsilon_{z0}\epsilon_{cr}\epsilon_{L3}\epsilon_{trg}\epsilon_T$ in expression for ϵ_Z is equivalent to the definition of ϵ_W according to the Equations 34 and 40. Canceling these parameters in the ratio we obtain

$$\epsilon_Z/\epsilon_W = \epsilon_Z^{cr}\epsilon_L[1 + f(1 - \epsilon_{trg}\epsilon_{rec}\epsilon_{dx})]/\epsilon_W^{cr}. \tag{52}$$

We use the efficiency numbers from Table 10 and Equations 31–37 to calculate the numeric value for the efficiency ratio

$$\epsilon_Z/\epsilon_W = 0.957^{+0.007}_{-0.011}\ . \tag{53}$$

12 Result

We wish to measure product of the production cross section and the branching ratio for a vector boson decay

$$\sigma(p\bar{p} \to V) \cdot BR(V \to \mu X) = \frac{N(1-b)}{A\epsilon \int L\,dt}, \tag{54}$$

where: N — the number of candidate events passing the selection, b — the estimated fraction of background events, A — detector acceptance, ϵ — efficiency of the selection cuts, $\int Ldt$ — luminosity integral.

Alternatively, we can combine our sensitivity to both W and Z decays to measure a luminosity independent cross section ratio

$$R = \frac{\sigma(p\bar{p} \to W) \cdot BR(W \to \mu\nu)}{\sigma(p\bar{p} \to Z) \cdot BR(Z \to \mu\mu)} = \frac{N_W(1-b_W)}{N_Z(1-b_Z)}\frac{A_Z}{A_W}\frac{\epsilon_Z}{\epsilon_W}\ . \tag{55}$$

The measured input parameters for these calculations 54–55 summarizing all the analysis presented here are shown in table 11. For many parameters systematic uncertainties are quoted next to the central values.

Parameter	W	Z	Ratio R
Integrated Luminosity	$\int L\,dt$ 193.5±11.6 pb^{-1}	$\int L\,dt$ 193.5±11.6 pb^{-1}	
Number Of Candidates	N_W 57,109	N_Z 3,568	$\frac{N_W}{N_Z}$ 16.006
Background Fraction	b_W 0.0949±0.0045	b_Z 0.0036±0.0019	$\frac{1-b_W}{1-b_Z}$ 0.908±0.005
Acceptance	A_W $0.1451^{+0.0020}_{-0.0024}$	A_Z $0.1153^{+0.0021}_{-0.0026}$	$\frac{A_Z}{A_W}$ $0.7949^{+0.0068}_{-0.0076}$
Efficiency	ϵ_W $0.661^{+0.009}_{-0.010}$	ϵ_Z $0.633^{+0.011}_{-0.015}$	$\frac{\epsilon_Z}{\epsilon_W}$ $0.957^{+0.007}_{-0.011}$

Table 11: Measured input parameters for the cross section and ratio calculations.

12.1 W Cross Section

Using the values from Table 11 for $p\bar{p} \to W \to \mu\nu$ process in expression 54 we obtain the following result

$$\sigma(p\bar{p} \to W)BR(W \to \mu\nu) = 2.786^{+0.065}_{-0.055}(\text{syst}) \pm 0.012(\text{stat}) \pm 0.166(\text{lum})\ \text{nb}\ , \quad (56)$$

which agrees well with the previous result based on 72 pb^{-1} of CDF Run II data [4]

$$\sigma(p\bar{p} \to W)BR(W \to \mu\nu) = 2.791^{+0.077}_{-0.072}(\text{syst}) \pm 0.019(\text{stat}) \pm 0.167(\text{lum})\ \text{nb}\ . \quad (57)$$

To make a comparison with the theoretical prediction we use the calculated W production cross section for $p\bar{p}$ collisions at $\sqrt{s}$ =1.96 TeV [18]. The theoretical prediction of the cross section and the branching ratio product is:

$$\sigma(p\bar{p} \to W) \cdot BR(W \to \mu\nu) = 2.687 \pm 0.054\ \text{nb}, \quad (58)$$

where the uncertainties come from the next-to-next-to leading order splitting functions, parton distribution functions and from the electroweak parameters [19].

Figure 17 shows the results of W production cross section measurement in the leptonic channel from various experiments in comparison with the theoretical prediction.

12.2 Z Cross Section

In case of $p\bar{p} \to Z \to \mu^+\mu^-$ process we account for $\gamma^* \to \mu^+\mu^-$ admixture to the $Z \to \mu^+\mu^-$ decay by multiplying the number of Z signal events by a correction factor:

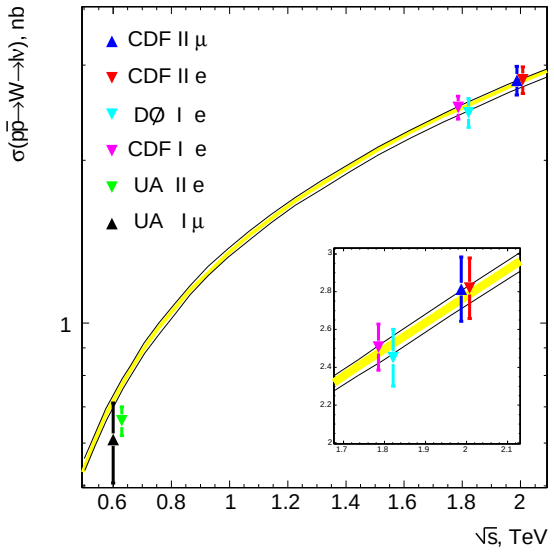

Figure 17: The measurements of W production cross section in leptonic channel.

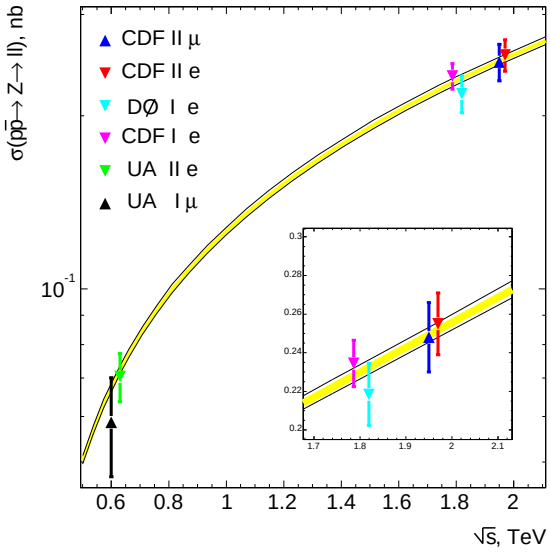

Figure 18: The measurements of Z production cross section in leptonic channel.

$$F_{Z\gamma^*} = \int_0^{\infty} \frac{d\sigma_Z}{dM_{\mu\mu}} dM_{\mu\mu} \Big/ \int_{66}^{116} \frac{d\sigma_Z + d\sigma_{Z\gamma^*} + d\sigma_{\gamma^*}}{dM_{\mu\mu}} dM_{\mu\mu} = 1.004 \pm 0.001 \ . \tag{59}$$

By using this factor we convert the measured $Z/\gamma^* \to \mu^+\mu^-$ cross section over the $66 - 116\text{GeV}/c^2$ dimuon invariant mass range to an exclusive $Z \to \mu^+\mu^-$ cross section over the entire dimuon invariant mass range.

Using the values from table for $p\bar{p} \to Z \to \mu^+\mu^-$ process in expression 54 we obtain the following result

$$\sigma(p\bar{p} \to Z)BR(Z \to \mu^+\mu^-) = 253.1^{+8.3}_{-6.4}(\text{syst}) \pm 4.2(\text{stat}) \pm 15.2(\text{lum}) \text{ pb} \ , \tag{60}$$

which agrees well with the previous result based on 72 pb^{-1} of CDF Run II data [4]

$$\sigma(p\bar{p} \to Z)BR(Z \to \mu^+\mu^-) = 253.1^{+8.9}_{-8.1}(\text{syst}) \pm 6.8(\text{stat}) \pm 15.1(\text{lum}) \text{ pb} \ . \tag{61}$$

To make a comparison with the theoretical prediction we use the calculated Z production cross section for $p\bar{p}$ collisions at $\sqrt{s}$ =1.96 TeV [18]. The theoretical prediction of the cross section and the branching ratio product is:

$$\sigma(p\bar{p} \to Z) \cdot BR(Z \to \mu^+\mu^-) = 251.3 \pm 5.0 \text{ pb}, \tag{62}$$

where the uncertainties come from the next-to-next-to leading order splitting functions, parton distribution functions and from the electroweak parameters [19].

Figure 18 shows the results of Z production cross section measurement in leptonic channel from various experiments in comparison with the theoretical prediction 18.

12.3 W/Z Cross Section Ratio

To calculate the cross section ratio we use the expression 55 with the parameter values from table 11. We multiply the number of Z candidates by the correction factor $F_{Z\gamma^*}$ as described in the previous subsection and obtain the following result:

$$R = 11.02^{+0.17}_{-0.14}(\text{syst}) \pm 0.18(\text{stat}) \ , \tag{63}$$

which agrees well with the previous result based on 72 pb^{-1} of CDF Run II data [4]

$$R = 11.03 \pm 0.18(\text{syst}) \pm 0.31(\text{stat}) \ . \tag{64}$$

The cross section ratio result 63 has significant improvement in precision over the cross section measurements of W 56 and Z 60 for which luminosity is a considerable source of uncertainty. In addition, the acceptance and efficiency calculation errors contribute less when used in the ratio due to the full or partial cancellations of uncertainty sources as can be seen in table 11.

To make a comparison with the Standard Model prediction we use the calculated ratio of W and Z production cross section for $p\bar{p}$ collisions at $\sqrt{s}$ =1.96 TeV [18]. The theoretical prediction of the ratio 55 is:

$$R = 10.69 \pm 0.013 \ , \tag{65}$$

where the uncertainties come from the next-to-next-to leading order splitting functions, parton distribution functions and from the electroweak parameters [19].

12.4 Extracting Physics Quantities

Equation for the cross section ratio 2 can be rewritten to express the W leptonic branching ratio:

$$BR(W \to \mu\nu) = \frac{\sigma(p\bar{p} \to Z)}{\sigma(p\bar{p} \to W)} \cdot BR(Z \to \mu\mu) \cdot R \ , \tag{66}$$

where the measured value of R is our result 63.

The Standard Model prediction for the W and Z production cross section ratio is:

$$\frac{\sigma(p\bar{p} \to W)}{\sigma(p\bar{p} \to Z)} = 3.3677 \pm 0.0155 \ , \tag{67}$$

according to the theoretical calculations [18] and [19].

For Z leptonic branching ratio we take the world average value [5]

$$BR(Z \to \ell^+\ell^-) = 3.3658 \pm 0.0023 \ \%. \tag{68}$$

To obtain the value for our indirect measurement of W leptonic branching ratio we put parameters 63, 67 and 68 in the Equation 66:

$$BR(W \to \mu\nu) = 11.01^{+0.17}_{-0.14}(\text{syst}) \pm 0.18(\text{stat}) \pm 0.05(\text{ext}) \ \%, \tag{69}$$

where the external error comes from the input uncertainties of Equations 67–68. Figure 19 shows the comparison of our result for W leptonic branching ratio with those from the other measurements and the Standard Model prediction. The Standard Model value [14] is 10.82±0.02 %. The world average value is 10.68±0.12 %, which is based on 2002 edition of the Review of Partivle Physics [5] and includes Run I results.

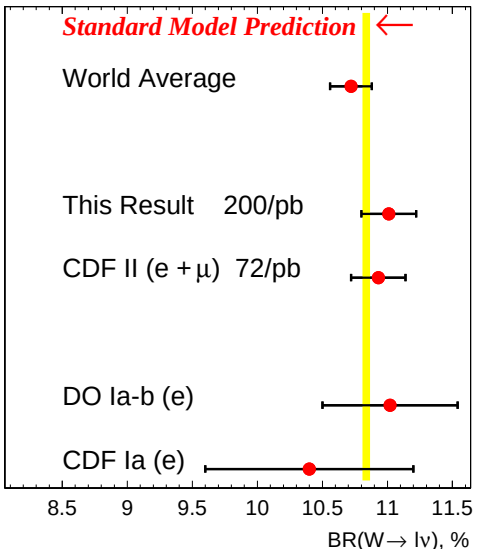

Figure 19: Comparison of our result for $BR(W \to \ell\nu)$ with those from the other measurements and the Standard Model expectation.

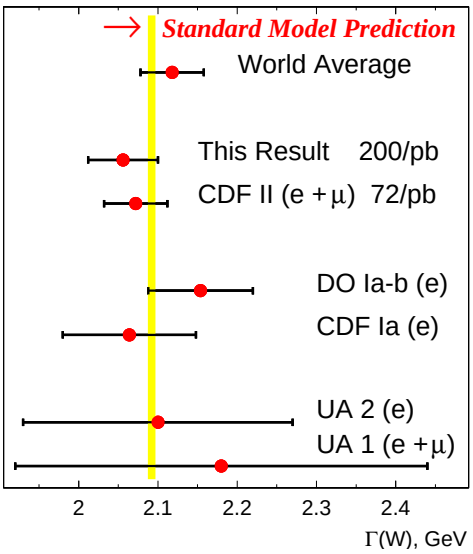

Figure 20: Comparison of our result for $\Gamma(W)$ with those from the other measurements and the Standard Model prediction.

We can extract the value for the full width of W if we take the Standard Model value [5] for W lepton partial width

$$\Gamma(W \to \ell\nu) = 226.4 \pm 0.3 \text{ MeV}, \tag{70}$$

and divide it by our value for W leptonic branching ratio 69. The extracted value of W width is

$$\Gamma(W) = 2056^{+26}_{-32}(\text{syst}) \pm 34(\text{stat}) \pm 10(\text{ext}) \text{ MeV}, \tag{71}$$

where the external error comes from the input uncertainties of Equations 67–68 and 70. Figure 20 shows the comparison of our result for the full width of W with those from the other measurements and the Standard Model prediction. The Standard Model value [14] is 2092.1±2.5 MeV. The world average value is 2118±42 MeV, which is based on 2002 edition of the Review of Particle Physics [5] and includes Run I results.

Acknowledgments

We would like to thank the conveners of CDF Electroweak Physics Working group A. Kotwal, P. Murat and D. Waters for many valuable feedbacks and fruitful discussions. We also wish to thank W. Sakumoto for providing this analysis with various parameters from theoretical calculations.

References

[1] Ken Bloom, Eric James, Jian Kang, Victoria Martin, Tracey Pratt, Michael Schmitt, Anyes Taffard, and Alexei Varganov, *Measurement of* $\sigma(p\bar{p} \to W \to \mu\nu)$ *with Data from CDF II*, CDF Note **6017**, Jul. 16, 2002. 2

[2] Ken Bloom, Eric James, Jian Kang, Victoria Martin, Tracey Pratt, Michael Schmitt, Anyes Taffard, and Alexei Varganov, *Measurement of* $\frac{\sigma(p\bar{p}\to W\to\mu\nu)}{\sigma(p\bar{p}\to Z\to\mu^+\mu^-)}$ *with Data from CDF II*, CDF Note **6025**, Jul. 10, 2002. 2

[3] Ken Bloom, Eric James, Jian Kang, Victoria Martin, Michael Schmitt, Anyes Taffard, and Alexei Varganov *Updated Measurements of* $\sigma(p\bar{p} \to W \to \mu\nu)$, $\sigma(p\bar{p} \to Z \to \mu\mu)$, *and R Using CDF Run II Data*, CDF Note **6302**, Mar. 21, 2003. 2

[4] Dan Amidei, Ken Bloom, Mircea Coca, Eva Halkiadakis, Eric James, Jian Kang, Young-Kee Kim, Giulia Manca, Victoria Martin, Pasha Murat, Aidan Robson, Willis Sakumoto, Michael Schmitt, Greg Veramendi, and Alexei Varganov *Measurements of* $p\bar{p} \to W \to \mu\nu$ *and* $p\bar{p} \to Z \to \mu\mu$ *Production Cross Sections and R Using CDF Run II Data*, CDF Note **6711**, Feb. 27, 2004. 2, 3, 18, 23, 26, 30, 31, 32

[5] K. Hagiwara et al. *Particle Data Group*, *Phys. Rev.* **D 66** (2002) 010001 3, 13, 15, 32, 33

[6] Data Quality Monitoring Group *Version IV of the Good Run List* `http://www-cdf.fnal.gov/internal/dqm/goodrun/v4/goodv4.html` 3

[7] Ricardo Eusebi *Secondary Data Sets for the Top Group* `http://b0urpc.fnal.gov/~eusebi/Stripping/TopDataSets.html` 3

[8] Evelyn J. Thomson *Description of data samples for Top Group for Summer 2003*, CDF Note **6548**, Jul. 1, 2003. 3, 26

[9] Dmitry O. Litvintsev *The CDF Run II Data File Catalog,* CDF Note **5983**, May. 29, 2002. 3

[10] Torbjörn Sjöstrand, Leif Lönnblad, Stephen Mrenna, Peter Skands *PYTHIA 6.3 Physics and Manual,* `hep-ph/0308153` 3

[11] Daniel Stump, Joey Huston, Jon Pumplin, Wu-Ki Tung, H. L. Lai, Steve Kuhlmann, J. F. Owens *Inclusive Jet Production, Parton Distributions, and the Search for New Physics,* hep-ph/0303013 3

[12] Mircea Coca, Henry Frisch, David Goldstein, Jaco Konigsberg, Mark Kruse, Nancy Lai, Carla Pilcher, David Saltzberg, Paul Tipton, Un-ki Yang *Draft Proposal for the Summer-2002 Top Dilepton Analysis and Top Dilepton Dataset*, CDF Note **5676**, Jul. 13, 2001. 5

[13] Heather K. Gerberich, Ashutosh V. Kotwal and Chris Hays *Cosmic Ray Tagging using COT Hit Timing*, CDF Note **6089**, Aug. 19, 2002. 6

[14] Eva Halkiadakis, Eric James, Jian Kang, Guilia Manca, Victoria Martin, Pasha Murat, Peter Renton, Willis Sakumoto, Michael Schmitt, *Updated Combination of e and μ Measurements of the W and Z Cross Sections and Their Ratio*, CDF Note **6894**, Mar. 6, 2004. 15, 33

[15] The CDF Collaboration (F. Abe et al.), *A Measurement of the ratio $\sigma(p\bar{p} \rightarrow W)B(W \rightarrow e\nu)/\sigma(p\bar{p} \rightarrow Z^0)B(Z^0 \rightarrow e^+e^-)$ in $p\bar{p}$ collisions at $\sqrt{s}$ =1800 GeV*, Phys. Rev. *Phys. Rev.* **D 52** (1995) 2624. 20

[16] Eva Halkiadakis, Eric James, Jian Kang, Guilia Manca, Victoria Martin, Pasha Murat, Aidan Robson, Michael Schmitt *PDF Uncertainties for W and Z Cross Section Measurements*, CDF Note **6890**, Feb. 22, 2004. 24

[17] C. Chen, I. Cho, C. Hays, M. Herndon, J. Kraus, J. Kroll, T. Miao, P. Murat, R. OldeMan, J.C Yun, *Measurement of the Track Reconstruction Efficiency in the COT Using a MC Track Embedding Technique*, CDF Note **6394**, Jun. 14, 2002. 26

[18] Willis Sakumoto, *W/Z Cross Section Predictions for $\sqrt{s} = 1.96$ TeV*, CDF Note **6341**, Feb. 23, 2003. 30, 31, 32

[19] Willis Sakumoto, *W/Z Cross Section Predictions Errors for $\sqrt{s} = 1.96$ TeV*, CDF Note **6899**, Feb. 25, 2004. 30, 31, 32